# AMPLITUDE AND PHASE RECONSTRUCTION ISSUES IN SCATTERING SCANNING NEAR-FIELD OPTICAL MICROSCOPY

Denis TRANCĂ[1], Stefan STANCIU[2], Radu HRISTU[3], Cătălin STOICHIȚĂ[4], George STANCIU[5]

*Scattering scanning near-field optical microscopy has become in the past decade a powerful tool for high-resolution optical investigations. However, a deeper understanding of the signal detection, demodulation and reconstruction techniques is still required. In this paper we use the mathematical concept that forms the base for modulation/demodulation of the signal in an interferometric detection scheme to analyze the process of reconstruction of the wanted signal (its amplitude and phase).*

**Keywords**: near-field, optical microscopy.

## 1. Introduction

Scattering scanning near-field optical microscopy (s-SNOM) has become well-known in the past years for its capabilities of achieving optical information with nanoscale resolution from the investigated samples [1–3]. It uses a typical Atomic Force Microscope (AFM) probe with its tip laterally illuminated by a laser beam; such a system usually is able to perform simultaneous tapping-mode AFM and s-SNOM investigations [3]. Many applications have been found for this microscopy tool, including infrared spectroscopy [4] and dielectric function measurements with nanoscale resolution [5, 6]. Many studies confirmed that the optical resolution of s-SNOM is not limited by the optical wavelength but rather by the curvature radius of the probe's tip (which offers a resolution comparable to that of an AFM) [1, 7–9].

While it has many advantages, s-SNOM is affected by several drawbacks. The most important is the presence of the background signal [10, 11], which is due to the light which suffers one or multiple reflections between the shaft of the cantilever and the sample's surface and which finally reaches the detector. This background signal (viewed as noise) can be greater that the wanted signal and as a result a poor signal-to-noise ratio is obtained. The most efficient way to overcome

[1] University POLITEHNICA of Bucharest, Romania, email: denis.tranca@cmmip-upb.org
[2] University POLITEHNICA of Bucharest, Romania, email: stefan.stanciu@cmmip-upb.org
[3] University POLITEHNICA of Bucharest, Romania, email: hristu_radu@yahoo.com
[4] University POLITEHNICA of Bucharest, Romania, email: catalin.stoichita@dxis-net.com
[5] University POLITEHNICA of Bucharest, Romania, email: stanciu@physics.pub.ro

this drawback is to implement Higher Harmonic Demodulation (HHD) technique [12] and Pseudoheterodyne Detection (PD) interferometric scheme [11]. Therefore, the resulting signal which is detected by the detector will contain in the Fourier domain several main harmonic components located at the harmonics of the oscillation frequency $f_o$ of the probe; the side-bands around each main component contain as well harmonic components located at $nf_o \pm mM$, where $M$ is the oscillation frequency of a reference mirror (part of the PD detection scheme; for more information see [11]), and $n, m$ are positive integers. These last harmonic components located in the side-bands are less affected by the background signal and two successive harmonic components from these side-bands can be used for reconstruction of the amplitude and phase of the wanted signal. The signal components located at frequencies $nf_o \pm mM$ and $nf_o \pm (m+1)M$ can be imaged by means of lock-in amplifiers. However, HHD and PD introduce a series of modifications to the signal, therefore hindering the interpretation process of the reconstructed data because the detected signal differs from the original form of the wanted signal.

In the context of the Oscillating Point-Dipole Model (OPDM – the classical model which describes the interaction between the probe's tip, sample's surface and incoming light) [10], the present paper presents a novel approach (by means of mathematical analysis) for a theoretical description of the detected signal in s-SNOM. The results obtained by using this new approach demonstrate that single or even two successive spectral components detection is not sufficient for a comprehensive reconstruction of the original signal. This has a great importance in the process of understanding and interpreting the s-SNOM images.

## 2. Methods

### *2.1. Software simulations*

The Wolfram|Alpha online platform and the Matlab programming software have been employed to perform the calculations and simulations. More precisely, the integral functions required in the analysis of the harmonic components of the s-SNOM signal were calculated in the Wolfram|Alpha platform, which uses sophisticated mathematical algorithms for integral calculations [13]. The simulation of the s-SNOM signal, the image analysis and the graphical representation of the complex numbers were done in the Matlab platform. The virtual sample used for visual representations was created in Matlab as well, and it emulates a sample containing Pt square domains deposited on a Si substrate (Fig.1). Note that the $x$, $y$ and $z$ scales are not important here because the resolution is not the subject of this work.

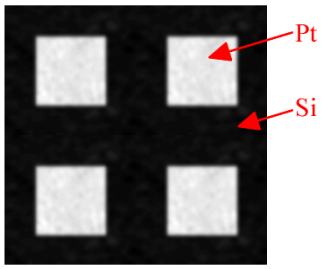


Fig. 1. Emulated sample containing Pt squares deposited on Si substrate

### *2.2. Mathematical model and calculations*

The mathematical model used in the present paper is OPDM; in this model, the probe's tip is treated as a nano-sphere in which an oscillating point-dipole is created by the electric field phasor $E_o$ associated with the external laser beam. This oscillating dipole interacts with the sample and emits light (with the same frequency as the incident electric field phasor $E_o$) that contains information related to the local optical properties of the sample. This light gives the wanted signal in s-SNOM. The electric field phasor of the light emitted by the oscillating dipole is usually known as the near-field phasor and this designation will be used in the following.

It is necessary to remind that the near-field phasor, $R$, can be mathematically modeled by complex representation and can be fully described either by its amplitude (modulus) and phase ($|R|$ and $\varphi$, respectively), or by its orthogonal projections ($X$ and $Y$):

$$R = |R| \cdot \exp(j\varphi) = |R| \cdot \cos(\varphi) + j \cdot |R| \cdot \sin(\varphi) = X + j \cdot Y \tag{1}$$

Thus, regardless of the way a complex number is described, two parameters are always needed.

In a regular s-SNOM setup working in a PD scheme, the two orthogonal projections can be recomposed from two successive harmonic components located in the side-bands of the main harmonics of the cantilever's oscillation frequency, i.e. $nf_o+mM$ and $nf_o+(m+1)M$. This can be done using a lock-in amplifier working on two separate channels. It's obvious from Eq. (1) that it is not sufficient to use a single signal channel for the lock-in amplifier (and thus detect only the $X_n$ or the $Y_n$ projection of the signal) to obtain quantitative (and even qualitatively correct) description of the sample. This will be exemplified in the Results section.

Going deeper into the problem, we should remind that the total near-field phasor is composed from a number of Fourier components [11]:

$$R = \sum_n \left|R_n\right| \cdot \exp\left(j\varphi_n\right) \tag{2}$$

If we choose to detect the signal from the second harmonic frequency, we use $n_2=2$ and $m=1$ and we obtain only the $X_2$ and $Y_2$ orthogonal projections of the component of order 2 – which may be very different from the orthogonal projections of the total near-field phasor.

In a rigorous representation, the total amplitude and phase of the near-field phasor will be, respectively:

$$\left|R\right| = \sqrt{R \cdot R^*} = \sqrt{\left(\sum_n X_n\right)^2 + \left(\sum_n Y_n\right)^2} \tag{3}$$

$$\tan\left(\varphi\right) = \frac{\sum_n Y_n}{\sum_n X_n} \tag{4}$$

It is obvious from Eq. (3) and (4) that each harmonic component contributes to the total amplitude and phase of the near-field phasor. Thus, a single complex component is not sufficient to obtain the whole information about the near-field phasor. This will be exemplified as well in the Results section.

The individual harmonic components can be calculated starting from the equations which describe the harmonic components of the near-field phasor ($c_n$) and those of the reference signal ($\rho_m$) [9]:

$$c_n = \alpha\left(\beta+1\right) \cdot E_o \cdot \frac{1}{2\pi} \cdot \int_{-\pi}^{\pi} e^{-j \cdot n \cdot u} \Bigg/ \left\{\left[\left(a+d_O+\frac{1}{2}\cdot z_O \cdot \sqrt[3]{\frac{16\pi}{\alpha\cdot\beta}}\right)+\frac{1}{2}\cdot z_O \cdot \sqrt[3]{\frac{16\pi}{\alpha\cdot\beta}}\cdot\sin(u)\right]^{-3} - 1\right\} du \tag{5}$$

$$\rho_m = J_m\left(\frac{2\pi}{\lambda}A\right) \cdot \rho \cdot \exp\left(j \cdot \psi_R + j \cdot m\frac{\pi}{2}\right) \tag{6}$$

In the equations above, $\alpha$ is the polarizability of the nano-sphere, $\beta$ is the reflection coefficient, $a$ is the radius of curvature of the tip, $d_o$ is the minimum tip-sample gap, $z_o$ is the oscillation amplitude of the probe, $J_m$ is the Bessel function of $m$ order, $A$ is the oscillation amplitude of the reference mirror, $\lambda$ is the wavelength of the incident laser beam, and $\psi_R$ is the mean phase difference between the interferometric pathways.

The orthogonal projections of the near-field phasor will be [11]:

$$X_n = 2 \cdot \left(real\left\{c_n\right\} \cdot real\left\{\rho_2\right\} + imag\left\{c_n\right\} \cdot imag\left\{\rho_2\right\}\right) \Big/ J_2\left(\frac{2\pi}{\lambda}A\right) \tag{7}$$

$$Y_n = 2 \cdot \left(real\left\{c_n\right\} \cdot real\left\{\rho_1\right\} + imag\left\{c_n\right\} \cdot imag\left\{\rho_1\right\}\right) \Big/ J_1\left(\frac{2\pi}{\lambda}A\right) \tag{8}$$

## 3. Results

The parameters involved in the calculations were as following: beam wavelength, λ = 638 nm; oscillation frequency of the s-SNOM probe, $f_o$ = 60 kHz; amplitude of the probe's oscillation, $z_o$ = 50 nm; oscillation frequency of the reference mirror, $M$ = 800 Hz; oscillation amplitude of the reference mirror, $A$ = 400 nm; mean phase difference between the interferometric pathways, $\psi = \pi$; radius of curvature of the tip, $a$ = 30 nm. The dielectric function for Pt at 638 nm is $\varepsilon_{Pt} = -11.83 - 19.77\,j$ [14] and for Si is $\varepsilon_{Si} = 15.07 - 0.15\,j$ [14].

### *3.1. Detection of a single harmonic component*

To calculate individual harmonic components $X_n$ and $Y_n$, first the integral from eq. (5) needs to be calculated. To simplify the calculations, the integral can be split is other simpler integrals which can be easily computed. We use the following notations:

$$\begin{cases} \mathcal{A} = a + d_o + \frac{1}{2}\cdot z_o \cdot \sqrt[3]{\frac{16\pi}{\alpha\cdot\beta}} \\ \mathcal{B} = \frac{1}{2}\cdot z_o \cdot \sqrt[3]{\frac{16\pi}{\alpha\cdot\beta}} \end{cases} \tag{9}$$

We can also write:

$$e^{-jmu} = \left[\cos(u) - j\cdot\sin(u)\right]^n \tag{10}$$

Now, for the first three orders, *n = 1, 2* and *3*, the components $c_n$ from eq. 5 will become:

$$c_1 = \alpha(\beta+1)\cdot E_o \cdot \frac{1}{2\pi}\cdot\left[\int_{-\pi}^{\pi}\frac{\cos(u)}{\left[\mathcal{A}+\mathcal{B}\cdot\sin(u)\right]^3 - 1}du - j\cdot\int_{-\pi}^{\pi}\frac{\sin(u)}{\left[\mathcal{A}+\mathcal{B}\cdot\sin(u)\right]^3 - 1}du\right] \tag{11}$$

$$\begin{aligned} c_2 = \alpha(\beta+1)\cdot E_o \cdot \frac{1}{2\pi}\cdot\Bigg[&\int_{-\pi}^{\pi}\frac{\cos^2(u)}{\left[\mathcal{A}+\mathcal{B}\cdot\sin(u)\right]^3 - 1}du - 2j\cdot\int_{-\pi}^{\pi}\frac{\sin(u)\cos(u)}{\left[\mathcal{A}+\mathcal{B}\cdot\sin(u)\right]^3 - 1}du - \\ &\int_{-\pi}^{\pi}\frac{\sin^2(u)}{\left[\mathcal{A}+\mathcal{B}\cdot\sin(u)\right]^3 - 1}du\Bigg] \end{aligned} \tag{12}$$

$$c_3 = \alpha(\beta+1)\cdot E_o \cdot \frac{1}{2\pi}\cdot\left[\int_{-\pi}^{\pi}\frac{\cos^3(u)}{\left[\mathcal{A}+\mathcal{B}\cdot\sin(u)\right]^3-1}du - 3j\cdot\int_{-\pi}^{\pi}\frac{\sin(u)\cos^2(u)}{\left[\mathcal{A}+\mathcal{B}\cdot\sin(u)\right]^3-1}du - 3\cdot\int_{-\pi}^{\pi}\frac{\sin(u)^2\cos(u)}{\left[\mathcal{A}+\mathcal{B}\cdot\sin(u)\right]^3-1}du + j\cdot\int_{-\pi}^{\pi}\frac{\sin^3(u)}{\left[\mathcal{A}+\mathcal{B}\cdot\sin(u)\right]^3-1}du\right] \quad (13)$$

The integrals in Eq. (11)-(13) are much easier to be calculated; their primitives were computed by using the Wolfram|Alpha online platform, and the returned results were used in a Matab custom program to calculate the values of $c_1$, $c_2$ and $c_3$ for certain parameters of the system. These values were used for computing (in Matlab) the signals $X_n$ and $Y_n$ ($n$ = *1, 2* and *3*) given by Eq. (7) and (8).

For the simulations we used the image from Fig.1 in which optical information is embedded using the Matlab software (see Methods). Eq. (6) – (8) together with the results returned by the Wolfram|Alpha platform were used to simulate the s-SNOM images. The images corresponding to the signals $X_n$, $Y_n$, $R_n$ and $\varphi_n$ are combined to form a single image for each order $n$ (see Fig.2). In this way, the contrast variations (and even contrast inversion) between the Pt and Si areas in the four signals can be easily observed.

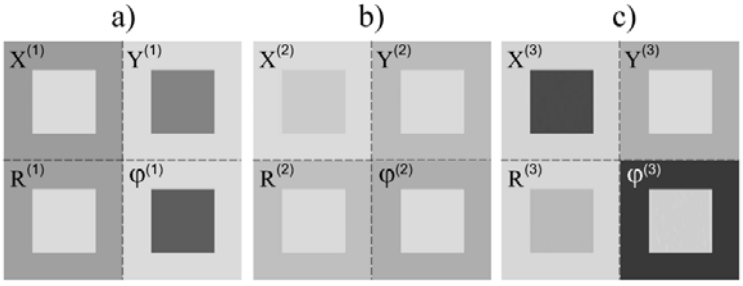


Fig. 2. Simulated s-SNOM images combining the signals $X_n$, $Y_n$, $R_n$ and $\varphi_n$ for the orders a) n=1; b) n=2; c) n=3

The differences in the contrast (revealed in Fig.2) prove that it is not possible to obtain quantitative optical information from a single orthogonal projection ($X_n$ or the $Y_n$). Not only that, but even a qualitative description is hard to obtain from a single orthogonal projection due to the contrast inversion which can occur between $X_n$ and $Y_n$. This happens as well if we look at the couple of signals $R_n$ and $\varphi_n$ or if we change the order $n$.

The results from the simulated s-SNOM images can be graphically represented and in Fig.3 there can be seen the representations of the phasors associated with each material (Pt and Si) for the three harmonic orders, n = 1 in Fig.3a, n = 2 in Fig.3b and n = 3 in Fig.3c. Fig.3 shows that if the measurements

are performed only on one axis (let say X), then the information from the other axis (Y) is lost.

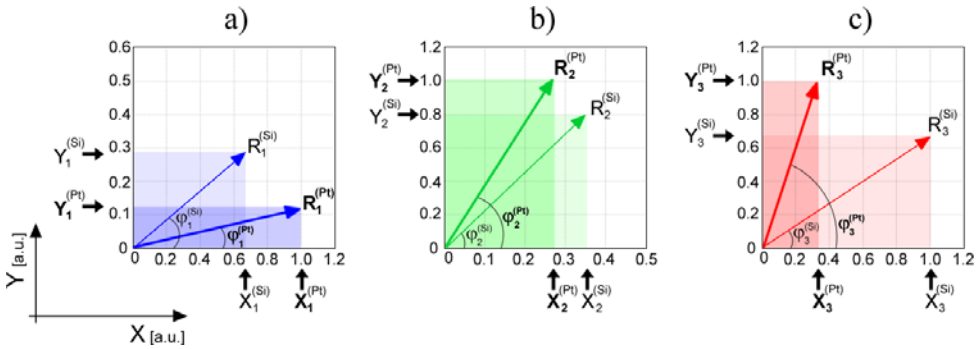


Fig. 3. Representations of the near-field phasors for the orders a) n=1; b) n=2; c) n=3

The image contrasts between the two materials (Pt and Si) can be calculated using the Michelson contrast formula [15, 16] for each image; the results are summarized in Table 1.

*Table 1*

| Contrast [%] | | | | | | | | | | | |
|---|---|---|---|---|---|---|---|---|---|---|---|
| $X_1$ | $Y_1$ | $R_1$ | $\varphi_1$ | $X_2$ | $Y_2$ | $R_2$ | $\varphi_2$ | $X_3$ | $Y_3$ | $R_3$ | $\varphi_3$ |
| 16.83 | -25.07 | 15.46 | -40.21 | -3.74 | 7.67 | 6.71 | 11.83 | -48.24 | 11.14 | -7.20 | 56.36 |

### *3.2. Detection of two successive harmonic components*

Computation of amplitude and phase requires two successive harmonic components detection for a certain order, $n$. However, even detection of two successive harmonic components to obtain $R_n$ and $\varphi_n$ can lead to incomplete description of the near-field phasor. This can be observed from Fig.2 and Fig.3 if one compares the contrasts between the three harmonic orders for amplitudes and phases. To avoid this, it is recommended to use Eq. (3) and (4) and calculate the sums in the equations for a greater order $n$. In this example we will use $n = 3$ (we use the first three orders just as a proof of concept, the computation being possible even for greater orders). Thus we obtain $R_{sum}$ (using Eq. 3) and $\varphi_{sum}$ (using Eq. 4).

However, the signal has several harmonic terms (more than three) and we want to compare $R_{sum}$ and $\varphi_{sum}$ with the amplitude and phase of the total near-field signal, $R_{NF}$ and $\varphi_{NF}$ respectively, which can be computed for the case when no modulations is performed. This can be done only theoretically; for an experimental case, there will always be the background signal which distorts the near-field signal.

We combine the images corresponding to the amplitudes $R_{sum}$ and $R_{NF}$, and the phases $\varphi_{sum}$ and $\varphi_{NF}$ (Fig.4). At this stage, two kinds of comparisons can be done.

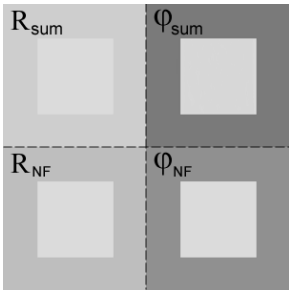


Fig. 4. Simulated s-SNOM images combining the amplitude and phase signals: $R_{num}$ (obtained from the first three orders), $R_{NF}$ (obtained from the total signal), $\varphi_{sum}$ (obtained from the first three orders) and $\varphi_{NF}$ (obtained from the total signal)

First, we observe that the amplitude $R_{sum}$ and phase $\varphi_{sum}$ images obtained by combining the signals from the first three orders are very different (in their contrast) from the images representing the amplitudes and phases for orders $n$ = 1, 2 and 3. This shows again that even if two successive spectral components are detected (for reconstruction of the amplitude and phase for a certain order $n$), the obtained information is not complete; a lot of information is lost because the harmonic components of other orders are not detected.

Secondly, we want to compare the image contrasts of amplitudes $R_{sum}$ and $R_{NF}$ (on one hand), and image contrasts of phases $\varphi_{sum}$ and $\varphi_{NF}$ (on other hand). Table 2 contains the values of these contrasts and we can observe that even detection of harmonic components for the first three orders is not sufficient to obtain the total information. However, depending on the application and the physical limitations of the experimental system, three orders detection may be appreciated as sufficiently close to the real situation. Of course, a near-field signal may have many harmonic components, but in practice is difficult to have too many lock-in amplifiers to simultaneously detect all the harmonic components.

*Table 2*

| Contrast [%] | | | |
|---|---|---|---|
| $R_{sum}$ | $R_{NF}$ | $\varphi_{sum}$ | $\varphi_{NF}$ |
| 3.95 | 6.05 | 27.43 | 20.39 |

## 4. Discussions

The presented results clearly show that detecting a single harmonic component in s-SNOM investigations is not sufficient because in this way only one orthogonal projection of the near-field phasors is obtained and the information contained in the other orthogonal projection is lost. A more critical situation is that when for two different materials the phasors associated to them have the same projection on one of the axis; in this case, if the detection is made only on that axis, no contrast will be observed between the two materials.

However, even detection on both axes can conduct to an incomplete description of the near-field phasors, as it can be seen from the results presented in Fig.4 and in Table 1. Best result can be obtained if several harmonic components are detected; as explained earlier, a signal may have many harmonic components and detection of all of them can be difficult to have in practice because of the need for several lock-in amplifiers, several imaging channels, etc. However, up to three harmonics can be sufficient for most of the applications; in particular cases, depending on the requirements of the application, more harmonic components can be added to improve the results.

## 5. Conclusions

In summary, an analysis of the signals detected in a PD s-SNOM scheme has been made. The results presented here point out that the detection of a single orthogonal projection of the near-field phasors can offer a distorted description of the near-field phasor. Even more, detection of both orthogonal projections can be insufficient if only a single harmonic component of the near-field phasor is imaged. The solution to this is to detect as much harmonic components of the signal as possible.

## Acknowledgements

The work is supported by the Sectoral Operational Programme Human Resources Development (SOP HRD), financed from the European Social Fund and the Romanian Government under the contract number POSDRU/159/1.5/S/137390/ (D. E. Tranca). The work of R. Hristu has been funded by the Sectoral Operational Programme Human Resources Development 2007-2013 of the Ministry of European Funds through the Financial Agreement POSDRU/159/1.5/S/132397. The presented work has been supported as well by the research grants PN-II-PT-PCCA-2011-3.2-1162.

## R E F E R E N C E S

[1]. *A.Horneber, K.Braun, J.Rogalski, P.Leiderer, A.J.Meixner, and D.Zhang*, "Nonlinear optical imaging of single plasmonic nanoparticles with 30 nm resolution", in Physical Chemistry Chemical Physics, 2015

[2]. *T.W.Johnson, Z.J.Lapin, R.Beams, N.C.Lindquist, S.G.Rodrigo, L.Novotny and S.H.Oh*, "Highly reproducible near-field optical imaging with sub-20-nm resolution based on template-stripped gold pyramids", in ACS Nano, **vol. 6**, no. 10, 2012, pp. 9168-9174

[3]. *C.Stoichita, R.Hristu, S.G.Stanciu and G.A.Stanciu*, "Near field investigation based on a novel apertureless near field optical microscope", in 3rd ICTON Mediterranean Winter Conference (ICTON-MW), 2009.

[4]. *Z.Nuño, B.Hessler, B.Heiberg, R.Damato, T.Dunlap, Y.S.Shon and Y.Abate*, "Nanoscale near-field infrared spectroscopic imaging of silica-shell/gold-core and pure silica nanoparticles", in Journal of Nanoparticle Research **vol. 14**, no. 3, 2012, pp. 1-8

[5]. *A.A.Govyadinov, S.Mastel, F.Golmar, A.Chuvilin, P.S.Carney and R.Hillenbrand*, "Recovery of permittivity and depth from near-field data as a step toward infrared nanotomography", in ACS Nano, **vol. 8**, no. 7, 2014, pp. 6911-6921

[6]. *D.E.Tranca, S.G.Stanciu, R.Hristu, C.Stoichita, S.Tofail, G.A.Sranciu*, "High-resolution quantitative determination of dielectric function by using scattering scanning near-field optical microscopy", in Scientific Reports, **vol. 5**, no. 11876, 2015, pp. 1-8

[7]. *R.Hillenbrand, F.Keilmann*, "Material-specific mapping of metal/semiconductor/dielectric nanosystems at 10 nm resolution by backscattering near-field optical microscopy", in Applied Physics Letters, **vol. 80**, no. 1, 2002, pp. 25-27

[8]. *F.Huth, A.Govyadinov, S.Amarie, W.Nuansing, F.Keilmann, R.Hillenbrand*, "Nano-FTIR absorption spectroscopy of molecular fingerprints at 20 nm spatial resolution", in Nano Letters, **vol. 12**, no. 8, 2012, pp. 3973-3978

[9]. *A.Bek, R.Vogelgesang, K.Kern*, "Apertureless scanning near field optical microscope with sub-10nm resolution", in Review of Scientific Instruments, **vol. 77**, no. 4, 2006

[10]. *B.Knoll and F.Keilmann*, "Enhanced dielectric contrast in scattering-type scanning near-field optical microscopy", in Optics Communications, **vol. 182**, no. 4, 2000, pp. 321-328

[11]. *N.Ocelic, A.Huber and R.Hillenbrand*, "Pseudoheterodyne detection for background-free near-field spectroscopy", in Applied Physics Letters, **vol. 89**, no. 10, 2006, pp. 101124:1-3

[12]. *N.Maghelli, M.Labardi, S.Patanè, F.Irrera and M.Allegrini*, "Optical near-field harmonic demodulation in apertureless microscopy", in Journal of microscopy, **vol. 202**, no. 1, 2001, pp. 84-93

[13]. *Wolfram Research, Inc.*, Mathematica, Version 10.1, Champaign, IL, 2015

[14]. *E.D.Palik* (*editor*), Handbook of optical constants of solids, Part II, Editura Academic Press, USA, 1985.

[15]. *E.Peli*, "Contrast in complex images", in JOSA A, **vol. 7**, no. 10, 1990, pp. 2032-2040

[16]. *D.E.Tranca, C.Stoichita, R.Hristu, S.G.Stanciu and G.A.Stanciu*, "A study on the image contrast of pseudo-heterodyned scattering scanning near-field optical microscopy", in Optics Express, **vol. 22**, no. 2, 2014, pp. 1687-1696